Results in Materials 8 (2020) 100147

Contents lists available at ScienceDirect

Results in Materials

journal homepage: www.journals.elsevier.com/results-in-materials

Effect of molybdenum, aluminium and boron on the phase transformation in 4 wt.–% manganese steels☆

A. Gramlich *, C. van der Linde, M. Ackermann, W. Bleck

Institut für Eisenhüttenkunde of RWTH Aachen University, Intzestrasse 1, 52072, Aachen, Germany

ARTICLE INFO

Keywords:
Ms-Temperature
Medium mananese steels
MLR
CCT-Diagram
Critical cooling rate

ABSTRACT

The transformation behavior of medium manganese steels after forging has been characterized using dilatometry in order to investigate the influence of the alloying elements. The alloys contain 4 wt.–% manganese, 0.5 wt.–% silicon, 0.035 wt.–% niobium and varying amounts of carbon (0.15–0.19 wt.–%), aluminum (0.025–0.5 wt.–%), molybdenum (0.02–0.2 wt.–%), titanium (0–0.02 wt.–%), and boron (0–0.06 wt.–%). The continuous cooling transformation (CCT) diagrams and a multiple linear regression (MLR) formula for calculating the martensite start (M_s) temperature is presented. The results are critically compared to a variety of formulae available in the literature. It is demonstrated within this study that molybdenum increases the M_s-temperature, silicon has no mandatory influence on the M_s-temperature and boron not only decreases the M_s-temperature but also increases the critical cooling rate. The new formula enables the precise setting of annealing parameters.

1. Introduction

Quench and tempering (Q + T) as well as precipitation hardening ferritic pearlitic (PHFP) steels represent the state of the art in the forging industry. Q + T steels are distinguished by their good balance of strength and toughness, while PHFP steels show inferior mechanical properties but are produced with a shorter thermomechanical process. The shortened process cuts the costs of these alloys by 25% in comparison to the Q + T steels [1,2]. Recently, air hardening medium manganese steels were developed and are now on the edge of industrial application [3–6]. These materials aim to combine the properties of Q + T steels with a process similar to PHFP steels. Additionally, these materials show cyclic material properties in the air cooled condition which exceed the values of Q + T in the tempered condition by 50%. The alloys [5] were designed for long products with inhomogeneous cross sections with diameters greater than 70 mm. Due to the rather complex geometries of these massive components the local cooling rates differ significantly. Therefore, a broad understanding of the transformation behavior, especially of the martensite transformation, is necessary in order to predict the influence of chemical variations caused by deviations of the industrial production.Since the fundamentals of the martensite formation were understood in the 1920s [7,8], an enormous amount of research was carried out on martensite in general and specificaly on the martensite transformation start temperature M_s. As this M_s does not correspond to the thermodynamic equilibrium temperature between martensite α' and austenite γ [9], M_s can not be calculated by simple thermodynamic calculations. Different strategies for predicting M_s-temperatures have been pursued in the past with multiple linear regression (MLR) equations [10–31], MLR with an additional factor like the austenitisation temperature (MLR+) [32–35], polynomial equations (PE) [10,36–38] and thermodynamic approaches (TDE) [39,40]. In recent years, neural networks were used to develop MLRs [11,41] using large datasets. However, the MLR equations are by far the most widespread method and are widely used by industry. MLR equation rely on the assumption that each element is influencing the M_s-temperature linearly (Equation (1)), while other approaches (PE) consider interactions between the different alloying elements.

$$M_s = c_0 + \sum_i c_i w_i \tag{1}$$

☆ Results presented here are from the research project IGF 27 EWN. Funding was provided by the German Federal Ministry of Economics and Energy via the German Federation of Industrial Cooperative Research Associations "Otto von Guericke" (AiF) in the program to encourage the industrial Community research by an resolution of the German Bundestag and the Steel Forming Research Society (FSV). The long version of the final report can be ordered after the end of the project from the FSV, Goldene Pforte 1, 58093 Hagen.

* Corresponding author.
E-mail addresses: alexander.gramlich@iehk.rwth-aachen.de (A. Gramlich), carina.van.der.linde@rwth-aachen.de (C. van der Linde), marc.ackermann@iehk.rwth-aachen.de (M. Ackermann), bleck@iehk.rwth-aachen.de (W. Bleck).

https://doi.org/10.1016/j.rinma.2020.100147
Accepted 21 September 2020
Available online 14 October 2020
2590-048X/© 2020 The Author(s). Published by Elsevier B.V. This is an open access article under the CC BY-NC-ND license (http://creativecommons.org/licenses/by-nc-nd/4.0/).

Table 1
Relevant element concentrations of the investigated alloys L1 - L5 and reference alloys R1-R2 [45], R3 - R4 [46] and R5-R8 [4], determined by spark emission spectrometry. All concentrations are given in wt.–%.

alloy	C	Si	Mn	Al	Cr	Mo	Ni	Ti	Nb	B
L1	0.19[a]	0.50	4.02	0.031	0.11	0.02	0.09	0.020	0.035	0.0016
L2	0.17[a]	0.50	3.99	0.025	0.11	0.02	0.10	0.020	0.033	0.0057
L3	0.15[a]	0.49	4.02	0.027	0.12	0.20	0.10	<0.003	0.035	<0.0005
L4	0.16[a]	0.52	4.00	0.510	0.11	0.21	0.10	<0.003	0.037	0.0030
L5	0.17[a]	0.50	3.96	0.027	0.12	0.02	0.10	<0.003	0.032	<0.0005
R1	0.42[a]	0.26	0.68	0.028	1.05	0.21	0.17	<0.001	<0.001	<0.0005
R2	0.45[a]	0.40	1.96	0.030	0.29	0.19	0.10	<0.001	<0.001	<0.0005
R3	0.25[a]	1.21	2.02	0.002	0.20	0.09	0.10	0.032	0.034	0.002
R4	0.26[a]	1.23	2.02	0.003	0.20	<0.002	0.10	0.032	0.034	0.001
R5	0.32[a]	0.16	3.00	0.026	0.10	0.02	0.10	<0.003	<0.005	<0.0005
R6	0.21[a]	0.16	6.55	0.025	0.10	0.02	0.11	<0.003	<0.01	<0.0005
R7	0.11[a]	0.15	9.94	0.021	0.11	0.02	0.10	<0.003	<0.01	<0.0005
R8	0.31[a]	0.15	9.85	0.020	0.11	0.01	0.10	<0.003	<0.01	<0.0005

[a] C determined with 'Leco' analyses.

Besides the determination of the start of the martensite transformation during continuous cooling the amount of formed martensite after cooling is of great importance. Koistinen and Marburger [42] defined the volume fraction of retained austenite after cooling to a specific temperature beyond M_s-temperature as displayed by Equation 2

$$V_y = \exp\left[-1.10 \cdot 10^{-2}\left(M_s - T_q\right)\right] \quad (2)$$

were V_γ gives the amount of retained austenite and T_q gives the temperature reached during quenching. Several authors re-used this equation and further modified it to calculate the volume fraction of formed martensite [31,43,44]. As it can be taken from the mathematical expression a microstructure of 100 vol–% martensite can theoretically not be reached. Therefore, other authors suggest a more technical approach to calculate the M_f-temperature by asuming that the temperature difference between M_s and M_f is constant [15,24,27]. The aim of this study is to investigate the phase transformation of different medium manganese steels during continuous cooling and the influence of alloying elements especially on the martensite transformation.

2. Experimental

Five alloys were laboratory cast (80 kg) and consecutively homogenized at 1200 °C for 5 h and finally forged at 1200°C into rods with a geometry of 60 x 60 x 1000 mm^3. The alloys differ concerning their carbon content (0.15 wt.–% to 0.19 wt.–%), aluminium content (0.025 wt.–% to 0.51 wt.–%), molybdenum content (0.02 wt.–% to 0.21 wt.–%), titanium content (0 wt.–% to 0.02 wt.–%) or their boron content (0 wt.–% to 0.0057 wt.–%). Manganese was alloyed to achieve a fully martensitic microstructure after air-cooling. Niobium was added to control the austenite grain size during forging. The different concentrations of aluminium, molybdenum, titanium and boron were chosen in order to prevent grain boundary embrittlement through manganese segregation. Detailed information about the microstructure and the mechanical properties can be found elsewhere [5]. The chemical composition is displayed in Table 1. Dilatometry was used to determine the transformation temperatures A_{cls}, A_{clf}, A_{c3}, M_s and M_f as well as for characterizing the transformation behavior during continuous cooling. For the experiments rectangular specimens (4.0 x 7.0 × 1.4 mm^3) and a dilatometer typ 'DIL-805A/D' of the company Texas Instruments were used. A_c-temperatures were characterized by heating to elevated temperatures using a heating rate of 0.05 K s^{-1}. M_s – and M_f-temperatures were characterized by three different experiments per alloy. Each specimen was heated to 950 °C using a heating rate of 3.33 K s^{-1}. Afterwards, the samples were quenched to room temperature with a cooling rate of 100 K s^{-1}. Continuous cooling transformation (CCT) diagrams were determined by performing 15 experiments per alloy. The heating rate was constant for all alloys 3.33 K s^{-1}, while the austenization temperature was chosen 50 K above A_{c3} for each alloy. After a holding time of 600 s the samples were continuously cooled to room-temperature with varying cooling rates for each curve. The determination of the obtained microstructure after cooling was done by optical microscopy (OM). Metallographic preparation was done by mechanical grinding with SiC paper up to 4000 grit followed by mechanical polishing using 3 m and 1 m diamond slurry. Subsequently, the samples were etched using nital-etching to reveal the microstructure.

Table 2
Through dilatometry determined transformation temperatures A_{c1}, A_{c1f}, A_{c3}, M_s and M_f for laboratory melts L1 - L5 and M_s for reference alloys R1 - R8. The A_c-temperatures for alloy R7 and R8 were not determinable with dilatometry.

$$\ln g_a = 9.81 - 4.62 \cdot w_c - 1.05 \cdot w_{Mn} - 0.50 \cdot w_{Cr} - 0.66 \cdot w_{Mo} - 0.54 \cdot w_{Ni} \quad (3)$$

$$\ln g_a = 16.00 - 4.62 \cdot w_c - 1.70 \cdot w_{Mn} + 4.00 \cdot w_{Al} - 0.50 \cdot w_{Cr} - 6.00 \cdot w_{Mo} - 0.54 \cdot w_{Ni} - 550 \cdot w_B \quad (4)$$

alloy	A_{c1}	A_{c1f}	A_{c3}	M_s	M_f
L1	665	731	792	309	144
L2	675	736	810	322	162
L3	660	724	806	348	167
L4	660	747	868	361	188
L5	662	728	802	328	159
R1	742	–	792	300	145
R2	710	–	800	266	–
R3	742	–	855	358	180
R4	711	–	850	368	173
R5	685	–	776	299	143
R6	571	–	736	238	86
R7	–	–	697	162	<RT
R8	–	–	–	68	<RT

3. Transformation behaviour during continuous cooling

The austenization during heating of this alloys is characterized by three transformation temperatures A_{cls}, A_{clf} and A_{c3}, where A_{clf} indicates complete dissolution of carbides. While A_{cls} only varies from 660 °C for alloys L3 and L4 to 675 °C for alloy L2, A_{clf} and A_{c3} show larger variations from 747 °C for alloy L1 to 806 °C for alloy L4 and from 792 °C for alloy L1 to 868 °C for alloy L4, respectively. The M_s – and M_f-temperatures, (not extracted from the CCT diagrams, but calculated through separately quenched samples) range from 309 °C to 361 °C and 144 °C to 188 °C. An overview of the identified transformation temperatures is displayed in Table 2. CCTs for alloys L1-L5 and additionally for a reference quench and tempering steel (42CrMo4) are displayed in Fig. 1. Further selected CCT-diagrams of reference alloys R5-R8 are added at the appendix (Figure A5). All laboratory melts show a shift of diffusion controlled

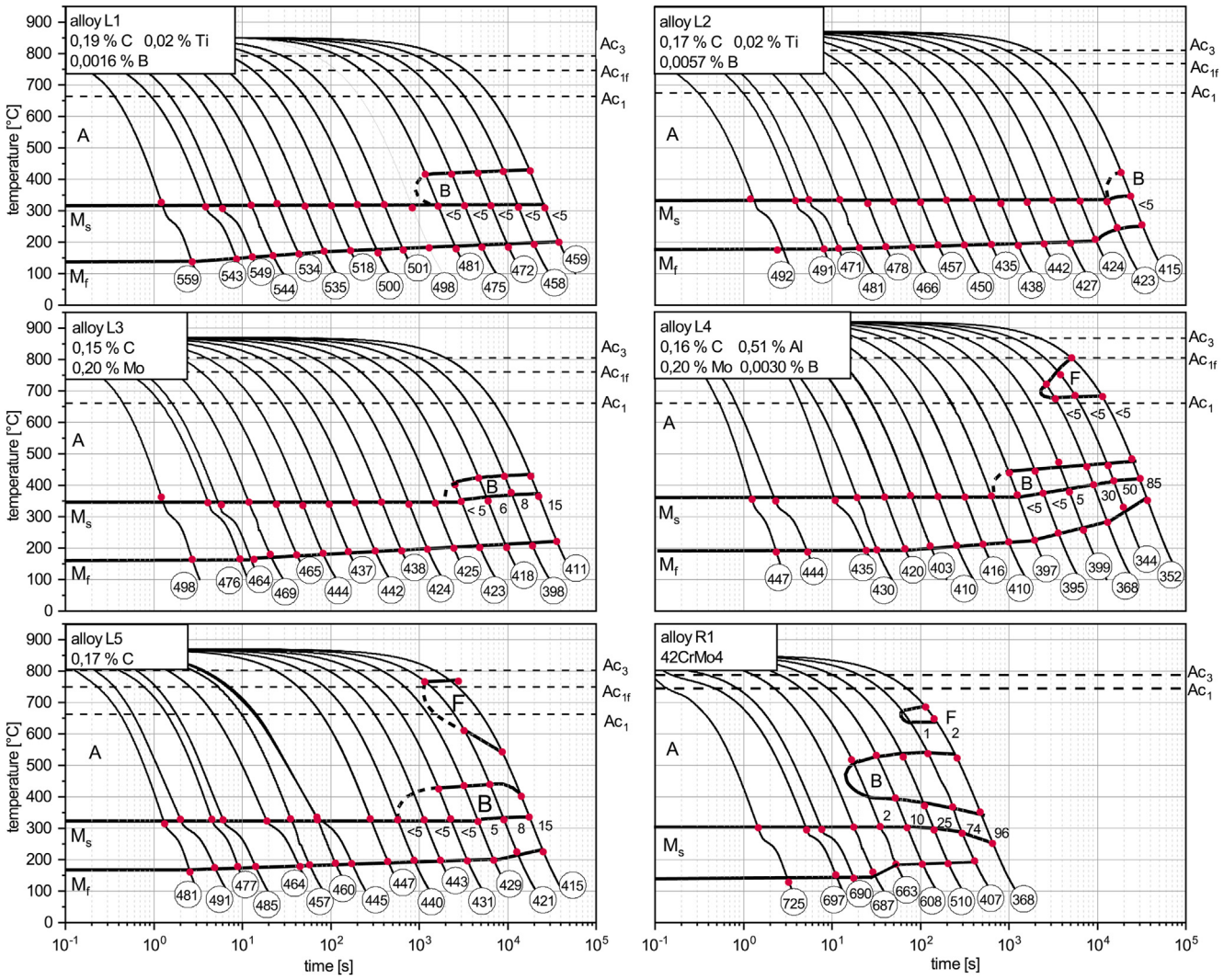

Fig. 1. Continous cooling diagrams for alloys L1-L5 and reference alloy 42CrMo4 (R1). Hardness is given in HV10.

phase transformations to longer times in comparison to the reference alloy. Alloy L5 shows a ferritic as well as a large bainitic phase field. With an increasing boron concentration, ferrite formation immediately gets suppressed while the bainite transformation is shifted to slower cooling rates (alloys L1 and L2). The M_s – and M_f-temperatures can be mainly explained by the small differences in carbon concentration. Interestingly, it is observed that the bainite start temperature decreases again for very small cooling rates. A comparison of the alloy L5 with the molybdenum (L3) and molybdenum + aluminium (L4) alloyed samples shows that the bainitic phase field is shifted to lower critical cooling rates, if molybdenum is alloyed. For the aluminium alloyed sample it was observed that the ferrite transformation range is shifted to higher temperatures and lower critical cooling rates in comparison to the reference alloy 42CrMo4. The critical cooling rate can be calculated by the empirical formula of Doane [47], which is shown in Equation (3). A comparison between the calculated and the measured critical cooling rates shows great discrepancies, as displayed in Fig. 2 a. As boron has a widely known effect on the hardenability the existing formula from Doane was amended by a factor for boron. Consecutively, the other factors were modified to achieve maximum congruence (compare Fig. 2b). The modified equation is displayed in Equation (4). For alloys R6-R8 only pure martensite microstructures were found even after very low cooling rates. These results are indicatedby the dashed lines. The right error bar represents the lowest cooling rates which was applied to these materials during this study.

4. Calculation of M_s-temperatures

In order to estimate the influencing elements and the range of their factors a large number of MLR needs to be evaluated as the elements and their factors change significantly in different literature sources (see Table 3). Fig. 3 shows an overview of 23 different MLRs. Only the relevant elemental factors for the investigated steels (carbon, manganese, silicon, aluminium, molybdenum, boron) and the initial parameter are listed. For each MLR the range of validity with respect to Mn is provided. Beside aluminium all elements reduce the M_s-temperature. For the impact of molybdenum only one study states that the M_s-temperature increases [11] by a Mo-addition while the majority of investigated studies state the opposite.

M_s-temperatures can be calculated by various approaches. In order to determine equations applicable for medium Mn steels different formulae were used to calculate the M_s-temperatures for the investigated alloys. Afterwards, the deviation between the calculated and the experimentally determined M_s-temperature was noted and the absolute value of the average deviation for each formula was listed. The results are summarized in Table 4. In order to reduce the potential equations, every equation with a deviation > 15 K was discarded. Only 3 non-MLR equations had a deviation > 15 K, two MLR + equations [34,35] and one thermodynamic approach [40]. In order to keep the calculation simple these methods were disobeyed as well. Especially the MLR + equations consider additional parameters like cooling rate which is

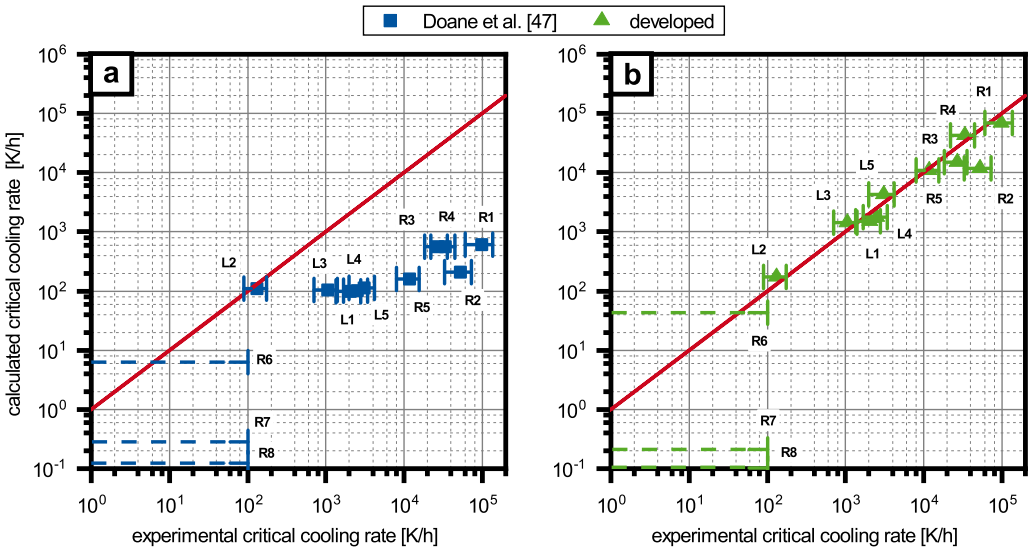

Fig. 2. Comparison of calculated and experimentally determined critical cooling rate. The experimental critical cooling rate is shown by the cooling rate where no bainite was found (right error bar) and the cooling rate were first bainite fractions where found (left error bar). The actual data point is in the middle of these two cooling rates. (a) shows the CCR based on the equation of Doane et al. [47] while (b) displays the results from the newly developed equation. For alloys R6-R8 no bainite was formed for the investigated cooling rates. Therefore, the longest applied cooling rate is shown (by the right error bar) and the experimental critical cooling rate is undetermined and represented by the dashed line.

applicable for flat products but difficult for long products. 7 equations with the deviation < 15 K were left for further consideration.

The formula of Li et al. [19] was designed on a set of alloys which included the alloy with the highest manganese concentration with up to 6,85 wt.–% manganese but only three out of 45 alloys have manganese concentrations above 3 wt.–%. Alloys with manganese concentration above 3 wt.–% are also underrepresented in the studies of Eichelman and Payson (Eichelman et al. [12] 2 out of 25; Payson et al. [24]: 2 out of 17). As the equation from Andrews is one of the most common formulae in literature and the investigated alloys have manganese concentration of up to 4,87 wt.–%, this formula was chosen for further optimization. Mahieu further optimized this formula by adding an aluminium factor to the equation which was also done in the present study. The complete formula of Andrews and Mahieu are shown in Equation (5) and Equation (6), respectively. The calculated M_s-temperature for the studied alloys is plotted against the measured M_s-temperature in Fig. 3. Since (a) displays the results obtained with equation of Andrews, (b) shows the results of the equation of Mahieu. While the calculated temperatures for alloy L3 and L4 appears to overlap with the measured ones, alloys L1, L2 and L5 show a positive aberrance of approximately 15 K. As the main difference between these groups is that L3 and L4 are alloyed with molybdenum, a positive factor was introduced and the initial parameter was reduced accordingly. Furthermore, a negative factor for boron was introduced and slight modifications of the residual parameters were done, resulting in Equation (7). The modified formula provides nearly perfect matches for calculated and experimentally determined temperatures, Fig. 3c.

$$M_s = 539 - 423 \cdot w_c - 30.4 \cdot w_{Mn} - 17.7 \cdot w_{Ni} - 12.1 \cdot w_{Cr} - 7.5 \cdot w_{Mo} \quad (5)$$

$$M_s = 539 - 423 \cdot w_c - 30.4 \cdot w_{Mn} - 7.5 \cdot w_{Si} + 30 \cdot w_{Al} \quad (6)$$

$$M_s = 517 - 423 \cdot w_c - 30.4 \cdot w_{Mn} + 82 \cdot w_{Mo} + 37 \cdot w_{Al} - 700 \cdot w_B \quad (7)$$

Table 3
Overview of different MLR formula [10–31] for calculating M_s-temperature. For each formula the factors of for carbon, silicon, manganese, aluminium molybdenum and boron are given, if they are included. C_0 of the formula of Capdevilla was modified for the usage of temperatures in °C. For each formula the range of manganese concentration of the steels which were used to develop the equations are given. More information about the different equations are summarized elsewhere [48].

Source	c_0	c_C	c_{Si}	c_{Mn}	c_{Al}	c_{Mo}	c_B	evaluated Mn Concentrations
Andrews [10]	539.0	−423.0		−30.4		−7.5		0,04-4,87
Capdevilla [11]	491.1	−302.6	−14.5	−30.6		2.4		−3,76
Eichelman-Hull [12]	811.6	−1666.7	−27.8	−33.3				0,63–5,03
Eldis [13]	531.0	−391.2		−43.3				0,35–1,80
Finkler-Schirra [14]	635.0	−474.0		−33.0		−21.0		0,16–1,35
Grange-Stewart [15]	537.8	−361.1		−38.9		−27.8		0,16–0,48
Jaffe-Hollomon [16]	550.0	−350.0		−40.0	30.0	−10.0		0,01–0,1
Kung-Rayment [17]	498.9	−300.0	−11.1	−33.3		−11.1		−2,1
Kunitake [18]	560.5	−407.3	−7.3	−37.8		−4.5		0,39–2,04
Li et al. [19]	540.0	−420.0	−10.5	−35.0	20.0	−21.0		0,29–6,85
Lotter I [20]	558.3	−312.0		−49.0				0,16–1,69
Lotter II [20]	452.6	−245.0		−8.1		−146.7		0,16–1,69
Mahieu et al. [21]	539.0	−423.0	−7.5	−30.4	30.0			1,54–1,56
Mikula-Wojnar [22]	635.0	−549.8	−69.0	−85.4		−69.3	−1746.5	–
Nehrenberg [23]	498.9	−300.0	−11.1	−33.3		−11.1		0,29–1,21
Payson-Savage [24]	498.9	−316.7	−11.1	−33.3		−11.1		0,30–4,87
Pickering [25]	502.0	−810.0		−13.0		−6.0		–
Rowland-Lylew [26]	498.9	−333.3	−11.1	−33.3		−11.1		0,31–0,50
Steven-Haynes [27]	561.1	−473.9				−21.1		0,44–1,38
Sverdlin-Ness [28]	520.0	−320.0	−5.0	−50.0		−20.0		−1,26
Tamura [29]	550.0	−361.0		−39.0	30.0	−5.0		–
Trzaska [30]	541.0	−401.0	−10.5	−36.0		−17.0		0,13–2,04
van Boehmen [31]	462.0	−273.0		−26.0		−30.0		0,002–0,69
Developed	517.0	−423.0		−30.4	37.0	82.0	−700.0	

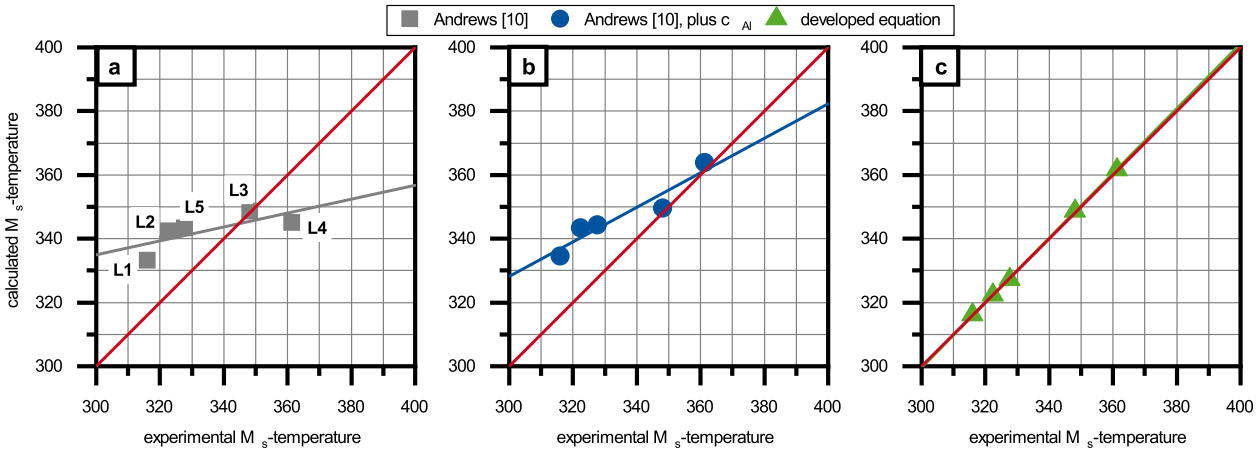

Fig. 3. Comparison of calculated and experimentally determined M_s-temperatures. (a) shows a standard equation from the literature (Andrews [10]) while (b) displays this equation with an additional coefficient for aluminium. (c) finally shows the newly developed equation.

5. Cooling rate dependency of M_f-temperatures

The martensite transformation is furthermore characterized by the martensite finish temperature M_f which is defined as the temperature during continous cooling where close to 100 vol–% of the austenite is transformed into martensite. While Koistinen and Marbuger state that there is theoretically no M_f temperature, technically this temperature can be defined as the temperature were no further measurable martensite is formed during cooling. As the temperature range (M_s â€“ M_f) therefore basically describes a process window which has to be crossed in order to form near to 100 vol–% marentsitic microstructures an estimation of the M_f temperature is necessary to design proper heat treatments. While most of the literature states constant values for the for the range M_f-M_s (Payson et al. [24]: M_s - 165 °C to 245 °C; Steven et al. [27]: 215 °C and Grange et al. [15] −104 °C) other studies indicate that this range may also be influenced by the chemical composition, for example by the concentration of nickel or manganese [24]. The investigated laboratory melts L1 to L5 show for the highest cooling rates differences between M_s and M_f between 160 K and 181 K for alloys L2 and L3 respectively. However, the question arises if more parameters can influence this process window. The CCT-diagrams indicate (Fig. 1) that the M_f-temperature is not constant for all cooling rates which is different to the observed behaviour of the M_s-temperature. Additionally, the measured hardness decreases significantly with decreasing cooling rate and increasing M_f temperature, even when no secondary phases were observed besides martensite. Therefore, the M_f-temperature can be calculated by Equation (8), where M_{f0} is the M_f-temperature after quenching with maximum cooling rate and $f(v_{cooling})$ is a function depending on mostly on cooling rate. As the increase of M_f is different for each investigated alloy, the assumption can be made that the composition of the alloys especially the carbon concentration and the concentration of elements which interact with carbon influence M_f as well.

$$M_f = M_{f0} + f\left(v_{cooling}\right) \tag{8}$$

Table 4
Discrepancies between calculated and experimentally determined Ms-temperatures for alloys L1-L5 and the average discrepancy. Different approaches were used to calculate the M_s-temperature: MLR [10–31], MLR+ [32–35], PE [10,36–38] and TDE [39,40] All discrepancies are in given in Kelvin.

Source	$M_s(L1)$	$M_s(L2)$	$M_s(L3)$	$M_s(L4)$	$M_s(L5)$	$\Delta\lvert\overline{M_s}\rvert$
Experimental	316	322	348	361	328	
Andrews [10]	333	343	349	345	343	14
Capdevila et al. [11]	300	307	312	310	308	28
Eichelman-Hull [12]	324	360	392	374	359	26
Eldis [13]	279	288	294	291	289	47
Finkler-Schirra [14]	406	417	421	417	417	81
Grange-Stewart [15]	306	314	315	312	315	22
Jaffe-Hollomon [16]	319	327	330	342	328	9
Kung-Rayment [17]	298	305	308	305	306	30
Kunitake [18]	322	331	337	334	332	11
Li et al. [19]	311	320	324	330	321	14
Lotter I [20]	286	294	312	310	308	33
Lotter II [20]	360	364	342	339	364	30
Mahieu et al. [21]	334	343	350	361	344	11
Mikula-Wojnar [22]	169	175	171	160	176	165
Nehrenberg [23]	298	305	308	305	306	30
Payson-Savage [24]	295	302	305	302	302	34
Pickering [25]	273	290	305	296	289	44
Rowland-Lylew [26]	291	299	302	300	300	37
Steven-Haynes [27]	467	477	482	477	476	141
Sverdlin-Nes [28]	250	257	258	256	259	79
Tamura [29]	321	329	334	346	330	9
Trzaska I [30]	313	322	326	322	323	14
van Boehmen [31]	302	308	307	305	309	29
Lee-Lee [32]	421	422	425	428	421	88
Lee-Park [33]	297	308	319	320	308	24
Trzaska II [34]	319	337	340	337	337	12
van Boehmen [35]	331	341	348	343	342	13
Andrews [10]	378	391	403	396	392	57
Carapella [36]	363	366	367	366	367	31
Liu et al. [37]	272	280	283	287	281	54
Miettinen I [38]	250	255	256	256	257	80
Miettinen II [38]	274	279	275	276	281	58
Cool-Bhadeshia [39]	297	313	317	294	325	26
Ghosh-Olson [40]	326	341	353	337	341	14

6. Discussion

The impact of the alloying content on the transformation behavior of medium Mn steels has been investigated and new formulae have been derived for the critical cooling rate, the martensite start temperature and the martensite finish temperature. This is relevant as the interaction of C and Mn in medium Mn steels affect segregation of C and precipitation of carbides and by this will change the transformation behavior.While formulae for M_s and M_f are of great interest for process design especially for quench and partitioning steels, the critical cooling rate in these steels is relevant for the control of bainite formation and in the present case for the successful suppression of the bainite formation. As Fig. 2 demonstrates, the new formula provides values with a significantly smaller deviation from the experimental measurements than the formula of Doane [47]. For forging components with large diameters the new formula provides a helpful tool to design the process, especially as the formula also predicts the critical cooling rates for the reference alloy 42CrMo4. As previously reported [45], the investigated alloys can be intercritically annealed to stabilize austenite to room temperature, which is a common procedure for medium manganese steels. During this heat

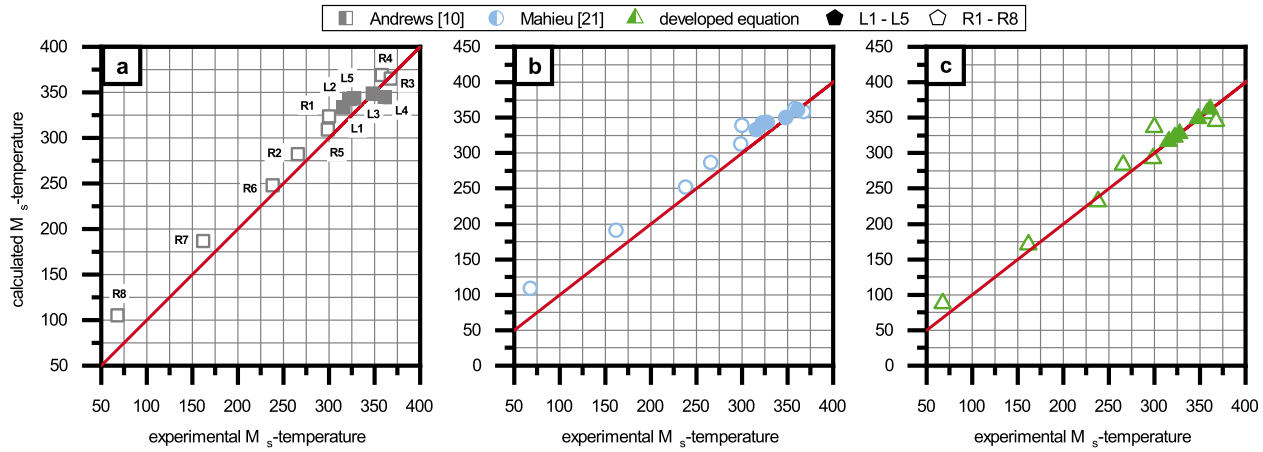

Fig. 4. Comparison of calculated and experimentally determined M_s-temperatures. For diagram (a) Andrew's equation, for diagram (b) Mahieu et al.'s equation and for diagram (c) the developed equation was used to calculate the M_s-temperatures.

treatment carbon and manganese enrich in the austenite regions and stabilize the γ-phase to room temperature. This partitioning can also take place during continuous cooling, when very small cooling rates are applied. The partitioning of carbon into the adjacent austenite is leading to a depletion of carbon in the residual matrix and therefore a reduction of the driving force for bainite formation, finally resulting in an austenite ferrite microstructure similar to microstructures after ART-annealing. This process gets intensified by the absence of boron or molybdenum which impede the diffusion, especially along grain boundaries and can therefore explain the decrease of the bainite start temperature of alloy L5 for very small cooling rates.The impact of different alloying elements on the M_s-temperature in steels has been extensively discussed in many publications, various empirical formulae for the quantification of the element-specific shift of M_s have been provided. Nevertheless, great accordance exists in the investigated literature that the influence of manganese on the M_s-temperature is negative, but more investigations on the class of medium manganese steels are required as the M_s-temperature for these alloys cannot be calculated precisely with available formulae [49]. The interaction between manganese and carbon lead to the retardation of carbon segregation and carbide precipitation which finally results in higher dissolved carbon in the matrix during cooling and lower M_s-temperature. It was demonstrated in other studies that the effect of manganese and carbon interaction can also influence mechanical properties like the hardness [50]. Additional reference alloys with varying contents of carbon, silicon and manganese were used to verify the developed formula. Fig. 4 displays the comparison of calculated and experimentally determined M_s-temperatures for the new formula (c) and for the formulae of Andrews [10] and Mahieu [21] (a-b). As it can be seen, the M_s-temperatures for these additional reference alloys can also be predicted by the new formula. The root mean square error of alloys L1-L5 is reduced to <1 K when using the new equation compared to 19 K and 14 K in the traditional equations. For the reference alloys R1-R8 the error is reduced to 18 K from 19 K to 24 K for Andrews and Mahieu, respectively. This results in an overall reduction for all investigated alloys

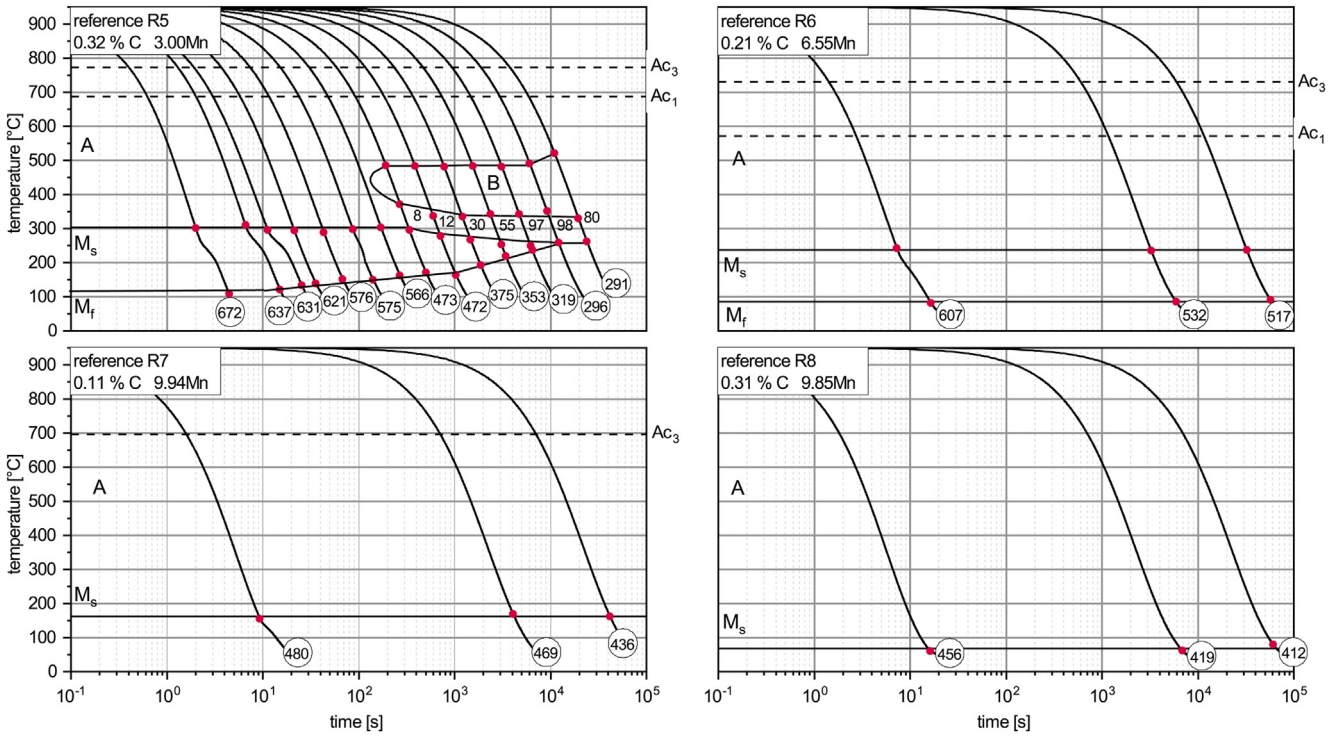

Fig. 5. Continous cooling diagrams for alloys R5-R8 [4]. Hardness is given in HV10.

to 14 K from 18 K to 21 K. The influence of boron is rarely found in the literature but Mikula et al. report a large negative factor (−1746,5) in their study. The size of the factor is not surprising as boron is known for its large influence on steels even when small amounts of this element is alloyed. As boron is interstitially dissolved in the austenite matrix it stabilizes the austenite phase and therefore decreases the M_s-temperature. As stated above, molybdenum was found to increase the M_s-temperature for the investigated steels and the formula also applies for the additional reference steels from Ackerman [46]. Most of the literature states that molybdenum decreases the M_s-temperature, but Capdevila et al. [11] demonstrated that molybdenum increases the M_s-temperature while using a neural network for the design of their MLR. Vermeulen et al. [41] investigated four different groups of medium carbon steels, also using a neural network. While three of his investigated alloy groups show an increase of the M_s-temperature until 0.5 wt.–% Mo only one group shows a negative trend with an increasing molybdenum concentration. The alloy group with the negative influence of molybdenum and one of the other groups were within the experimental deviation while the results of the remaining groups are believed to be statistical relevant. As the authors stated, main difference between these alloys is the carbon concentration which is 0.2 wt.–% for the alloys with the statiscally relevant molybdenum influence and 0.4 wt.–% for the other alloys. This indicates that the interaction of carbon and molybdenum might change with increasing carbon content, making the molybdenum influence negligible at high carbon concentrations. This could explain the deviation of 37K for alloy R1 which can be reduced to 19 K if the molybdenum influence is omitted. An explanation for the positive influence of molybdenum might be the interaction with carbon. The study from Hutchinson et al. [51] shows that even in ultrafast cooled martensite carbon already segregates to preferred sites at dislocations, phase boundaries or the vicinity of alloying elements. As molybdenum is a carbide forming element, molybdenum might act as a diffusion sink for nearby carbon which leads to a depletion of the surrounding matrix by carbon and therefore to an increase of the M_s-temperature. The schema that the M_s temperature of the alloys L3 and L4 are calculated lower than the residual alloys can be observed for several different equations from the literature, exemplary the equations from Grange et al. [15], Jaffe et al. [16] and Tamura et al. [29] demonstrating the independence of this observation from the equation of Mahieu et al. [21]. Assuming the linear relationship between the hardness of martensite and the carbon concentration [52], the decrease of hardness with decreasing cooling rate can be explained by a reduction of solute carbon in the matrix. During cooling with lower cooling rates diffusion is enabled after the first formation of martensite packets and carbon starts to form carbide predecessor phases or simply diffuses to lattice defects leading to a depletion of the dissolved matrix carbon concentration and finally to a reduced martensite hardness. The segregation of carbon and the resulting depletion of the matrix also explains the increase of M_f with decreasing cooling rates. While the material is cooled through the temperature range of martensite formation segregation of carbon and precipitation of carbides may occur that will affect the martensite transformation progress. For the description of the martensite temperature range of transformation a new schematic formula for the M_f has been derived that includes the applied cooling rate. However, more investigations on a broader database are required to determine all factors necessary to calculate M_f.

7. Conclusions

Medium Manganese Steels (MMnS) develop martensitic or bainitic microstructures even when very slow cooling rates are applied after hot forging. The impact of the alloying elements Mo, Al and B on the phase transformation has been investigated. An empirical equation for the martensite start temperature has been obtained and compared with literature data. The following conclusions can be drawn from this study:

- The addition of boron to MMnS retards the bainitic phase transformation, while Al promotes the ferrite and bainite formation.
- Surprisingly, molybdenum increases the martensite start temperature, which is contrary to most of the literature data. In MMnS, molybdenum might act as a diffusion sink for nearby carbon atoms which leads to a depletion of the surrounding austenitic matrix by carbon and therefore to a significant increase of the M_s-temperature. The M_f-temperature is hardly affected.
- The M_f-temperature is influenced by the cooling rate while the M_s stays constant until large volume fractions of bainite are formed. The increase of M_f is explained by the precipitation of carbide predecessor phases, leading to a depletion of carbon in the matrix.
- A new formula for the alloying impact on the M_s-temperature and the critical cooling rate have been derived by multiple linear regression. The new formula significantly improves the predictability of the martensitic transformation in MMnS.

Credit author statement

A. Gramlich, Conceptualization, Writing - original draft, Investigation, Visualization, Methodology. C. van der Linde, Formal analysis, Investigation, Visualization, Writing - review & editing. M. Ackermann, Writing - review & editing. W. Bleck, Writing - review & editing, Project administration, Funding acquisition.

Declaration of competing interest

The authors declare that they have no known competing financial interests or personal relationships that could have appeared to influence the work reported in this paper.

A. Appendix

B. Data availability

The raw/processed data required to reproduce these findings cannot be shared at this time as the data also forms part of an ongoing study.

References

[1] W. Bleck, M. Bambach, V. Wirths, A. Stieben, Microalloyed engineering steels with improved performance - an overview, HTM Journal of Heat Treatment of Materials 72 (2017) 346–354.
[2] W. Bleck, Werkstoffkunde Stahl für Studium und Praxis, 3. überarb. aufl. ed, Mainz, Aachen, 2010.
[3] A. Stieben, W. Bleck, S. Schönborn, Lufthärtender duktiler stahl mit mittlerem mangangehalt für die massivumformung, massivUmformung (2016) 50–55.
[4] A. Stieben, Eigenschaftenreport lufthärtender martensitischer Schmiedestähle mit Mangangehalten von 3-10 Gew.-%, Dissertation, RWTH Aachen University, Aachen, 16.03.18.
[5] A. Gramlich, T. Schmiedl, S. Schönborn, T. Melz, W. Bleck, Development of air-hardening martensitic forging steels, Mater. Sci. Eng., A 784 (2020) 139321.
[6] T. Schmiedl, A. Gramlich, S. Schönborn, T. Melz, Behaviour of Forging Steels under Cyclic Loading – the Benefit of Air-Hardening Martensites, Steel Research International, 2020.
[7] E.C. Bain, N.Y. Dunkirk, The nature of martensite, trans. AIME 70 (1924) 25–47.
[8] N. Seljakow, The nature of martensite, Nature 123 (1929) 204–205.
[9] E. Houdremont, O. Krisement, Arch. für das Eisenhuttenwes. 24 (1953) 53–68.
[10] K.W. Andrews, Empirical formulae for calculation of some transformation temperatures, Journal of The Iron and Steel Institute 203 (1965) 721–727.
[11] C. Capdevila, F.G. Caballero, C. García De Andrés, Determination of ms temperature in steels: a bayesian neural network model, ISIJ Int. 42 (2002) 894–902.
[12] G.H. Eichelmann, F.C. Hull, The effect of the composition on the temperature of spontaneous transformation of austenite to martensite, Transactions of American Society of Metals (1953) 77–95.
[13] J. Barralis, G. Maeder, Métallurgie: Tome 1: Métallurgie Physique, Communications actives, Paris, 1982.
[14] H. Finkler, M. Schirra, Transformation behaviour of the high temperature martensitic steels with 8 - 14% chromium, Steel Res. 67 (1996) 328–342.
[15] R.A. Grange, H.M. Stewart, The temperature range of martensite formation, Transactions of the American Institute of Mining and Metallurgical Engineers 167 (1946) 467–494.
[16] L.D. Jaffe, J.H. Hollomon, Hardenability and quench cracking, Transactions of the AIME 167 (1946) 617–646.

[17] C.Y. Kung, J.J. Rayment, An examination of the validity of existing empirical formulae for the calculation of ms temperature, Metall. Mater. Trans. 13 (1982) 328–331.
[18] T. Kunitake, H. Ohtani, Calculating the continuous cooling transformation characteristics of steel from its chemical composition, Sumitomo Search 2 (1969) 18.
[19] C. Li, et al., Computation of ms temperature in carbon equivalence method, J. Liaoning Tech. Univ. 17 (1998) 293–398.
[20] U. Lotter, Aufstellung von regressionsgleichungen zur beschreibung des umwandlungsverhaltens beim thermomechanischen walzen: Technical report, 1988.
[21] J. Mahieu, J. Maki, B.C. de Cooman, S. Claessens, Phase transformation and mechanical properties of si-free cmnal transformation-induced plasticity-aided steel, Metall. Mater. Trans. 33 (2002) 2573–2580.
[22] A.K. Lis, J. Lis, High strength hot rolled and aged microalloyed 5% ni steel, Journal of Achievements in Materials and Manufacturing Engineering 18 (2006) 37–42.
[23] A.E. Nehrenberg, Discussion, Transactions of the American Institute of Mining and Metallurgical Engineers 167 (1946) 494–501.
[24] P. Payson, C.H. Savage, Martensite reactions in alloy steels, Transactions of American Society of Metals 33 (1944) 261–280.
[25] F.B. Pickering, Physical metallurgical development of stainless steels, in: Stainless Steels '84', 1985, pp. 2–28. London.
[26] E.S. Rowland, S.R. Lyle, The application of ms points to case depth measurement, Transactions A.S.M. 37 (1946) 27–47.
[27] W. Steven, A.G. Haynes, The temperature formation of martensite and bainite in low-alloy steels, some effects of chemical composition, Journal of The Iron and Steel Institute 183 (1956) 349–359.
[28] A.V. Sverdlin, A.R. Ness, The effects of alloying elements on the heat treatment of steel, in: G.E. Totten (Ed.), Steel Heat Treatment Handbook, Dekker, New York, 1997, pp. 45–91.
[29] I. Tamura, Steel Material Study on the Strength, Nikkan Kogyo Shinbun Ltd., 1970.
[30] J. Trzaska, Calculation of critical temperatures by empirical formulae, Arch. Metall. Mater. 61 (2016) 981–986.
[31] S.M.C. van Bohemen, J. Sietsma, Effect of composition on kinetics of athermal martensite formation in plain carbon steels, Mater. Sci. Technol. 25 (2009) 1009–1012.
[32] S.-J. Lee, K.-S. Park, Prediction of martensite start temperature in alloy steels with different grain sizes, Metall. Mater. Trans. 44 (2013a) 3423–3427.
[33] S.-J. Lee, K.-S. Park, Prediction of martensite start temperature in alloy steels with different grain sizes, Metall. Mater. Trans. 44 (2013b) 3423–3427.
[34] J. Trzaska, Empirical formulae for the calculation of austenite supercooled transformation temperatures, Arch. Metall. Mater. 60 (2015) 181–185.
[35] S.M.C. van Bohemen, Bainite and martensite start temperature calculated with exponential carbon dependence, Mater. Sci. Technol. 28 (2012) 487–495.
[36] L.A. Carapella, Computing a" or ms (transformation temperature on quenching) from analysis, Metal Progress 46 (1944) 108.
[37] C. Liu, Z. Zhao, D.O. Northwood, Y. Liu, A new empirical formula for the calculation of ms temperatures in pure iron and super-low carbon alloy steels, J. Mater. Process. Technol. 113 (2001) 556–562.
[38] J. Miettinen, Simple semiempirical model for prediction of austenite decomposition and related heat release during cooling of low alloyed steels, Ironmak. Steelmak. 23 (1996) 346–356.
[39] T. Cool, H.K.D.H. Bhadeshia, Prediction of martensite start temperature of power plant steels, Mater. Sci. Technol. 12 (1996) 40–44.
[40] G. Ghosh, G.B. Olson, Kinetics of f.c.c. → b.c.c. heterogeneous martensitic nucleation—i. the critical driving force for athermal nucleation, Acta Metall. Mater. 42 (1994) 3361–3370.
[41] W.G. Vermeulen, P.F. Morris, A.P. de Weijer, A. van der Zwaag, Prediction of martensite start temperature using artificial neural networks, Ironmak. Steelmak. 23 (1996) 433–437.
[42] D.P. Koistinen, R.E. Marburger, A general equation prescribing the extent of the austenite-martensite transformation in pure iron-carbon alloys and plain carbon steels, Acta Metall. 7 (1959) 59–60.
[43] H.P. Hougardy, Description and control of transformations in technical applications, in: Steel: A Handbook for Materials Research and Engineering, Springer-Verlag, Berlin, 1992, pp. 167–200.
[44] S.-J. Lee, C.J. van Tyne, A kinetics model for martensite transformation in plain carbon and low-alloyed steels, Metall. Mater. Trans. 43 (2012) 422–427.
[45] A. Gramlich, R. Emmrich, W. Bleck, Austenite reversion tempering-annealing of 4 wt.% manganese steels for automotive forging application, Metals 9 (2019) 575.
[46] M. Ackermann, B. Resiak, P. Buessler, B. Michaut, W. Bleck, Effect of molybdenum and cooling regime on microstructural heterogeneity in bainitic steel wires, Steel Res. Int. 37 (2020) 1900663.
[47] D.V. Doane, J.S. Kirkaldy (Eds.), Hardenability Concepts with Applications to Steel, 1978. New York.
[48] A. Gorni, Steel Forming and Heat Treating Handbook, 2019, https://doi.org/10.13140/RG.2.1.1695.9764.
[49] S. Kaar, R. Schneider, D. Krizan, C. Béal, C. Sommitsch, Influence of the phase transformation behaviour on the microstructure and mechanical properties of a 4.5 wt.-% mn q&p steel, HTM Journal of Heat Treatment and Materials 74 (2019) 70–84.
[50] A. Gramlich, A. Stieben, M. Menzel, F. Pape, B. Lüneburg, W. Bleck, Manganese alloyed q & t steel with high hardenability for forging parts with large diameters, HTM Journal of Heat Treatment and Materials 74 (2019) 357–365.
[51] B. Hutchinson, J. Hagström, O. Karlsson, D. Lindell, M. Tornberg, F. Lindberg, M. Thuvander, Microstructures and hardness of as-quenched martensites (0.1–0.5% c), Acta Mater. 59 (2011) 5845–5858.
[52] R.A. Grange, C.R. Hribal, L.F. Porter, Hardness of tempered martensite in carbon and low-alloy steels, Metall. Mater. Trans. 8 (1977) 1775–1785.